5-21-2013

Photonically excited electron emission from modified graphitic nanopetal arrays

Patrick T. McCarthy
Birck Nanotechnology Center, Purdue University, pmccarth@purdue.edu

Scott J. Vander Laan
Birck Nanotechnology Center, Purdue University, svanderl@purdue.edu

David B. Janes
Birck Nanotechnology Center, Purdue University, janes@purdue.edu

Timothy S. Fisher
Birck Nanotechnology Center, Purdue University, tsfisher@purdue.edu

AIP | Journal of Applied Physics

Photonically excited electron emission from modified graphitic nanopetal arrays

Patrick T. McCarthy, Scott J. Vander Laan, David B. Janes, and Timothy S. Fisher

Citation: J. Appl. Phys. **113**, 193710 (2013); doi: 10.1063/1.4805038
View online: http://dx.doi.org/10.1063/1.4805038
View Table of Contents: http://jap.aip.org/resource/1/JAPIAU/v113/i19
Published by the AIP Publishing LLC.

Photonically excited electron emission from modified graphitic nanopetal arrays

Patrick T. McCarthy,[1,2] Scott J. Vander Laan,[1,3] David B. Janes,[1,3] and Timothy S. Fisher[1,2]
[1]*Birck Nanotechnology Center, Purdue University, West Lafayette, Indiana 47907, USA*
[2]*School of Mechanical Engineering, Purdue University, West Lafayette, Indiana 47907, USA*
[3]*School of Electrical and Computer Engineering, Purdue University, West Lafayette, Indiana 47907, USA*

(Received 11 February 2013; accepted 29 April 2013; published online 21 May 2013)

Efficient electron emission for energy conversion requires a low work function and a stable emitter material. The work function of graphene-based carbon materials can decrease significantly by intercalation with alkali metals, thus increasing their emission current. In this work, electron emission from potassium-intercalated carbon nanosheet extensions grown on electrode graphite is investigated. These petal-like structures, composed of 5–25 layers of graphene, are synthesized using microwave plasma chemical vapor deposition. Samples are intercalated with potassium, and a hemispherical energy analyzer is used to measure the emission intensity caused by both thermal and photonic excitation. The emission from the potassium-intercalated structures is found to consistently decrease the work function by 2.4 to 2.8 eV relative to non-intercalated samples. High emission intensity induced by photonic excitation from a solar simulator, with a narrow electron energy distribution relative to established theory, suggests that electron scattering decreases emitted electron energy as compared to surface photoemission. A modified photoemission theory is applied to account for electron scattering, and the sample work function and mean number of scattering events are used as parameters to fit theory to experimental data. The thermal stability of the intercalated nanopetals is investigated, and after an initial heating and cooling cycle, the samples are stable at low temperatures. [http://dx.doi.org/10.1063/1.4805038]

I. INTRODUCTION

Electron emission is the process by which electrons emit from one material into another material or medium, often a vacuum. Three main processes cause electron emission, and although they can occur simultaneously, historically they have been studied separately.[1] The first type, photoemission, occurs when an electron absorbs a photon with energy $\hbar\omega$; if the photon energy is greater than the work function, the electron can then overcome the potential barrier to leave the material.[2] Second, thermionic emission is similarly a classical mechanism in which the energy to overcome the barrier is gained through thermal excitation.[3] The third type, field emission, is a quantum-mechanical process where a high electric field is applied to the material in order to distort the potential barrier such that it is thin enough for electrons to tunnel through the barrier with non-negligible probability.[4] The present work considers the effects of photoemission from a carbon structure consisting of thin graphitic nanopetals decorating a graphitic surface that is particularly well suited for light absorption.

In recent years, carbon nanomaterials have been studied as possible electron emission sources. These materials have shown good emitter characteristics, and due to the unique bonding nature of carbon they can take a number of forms. Among the carbon nanomaterials studied are carbon nanofibers,[5] diamond films,[6] carbon nanotubes,[7] and more recently graphene.[8] The high mechanical strength and favorable electrical properties of these materials make them excellent candidates for field emission. The ability to fabricate low-dimensional carbon materials enables large field enhancement, and carbon nanotubes,[9,10] nanofibers,[11] and nanowalls[12] among others[13] have been studied. More recently, few-layer graphene nanosheets,[14] polymers of graphene[15,16] and single sheets of graphene[17] have been investigated. These materials are particularly attractive because they allow for large field enhancement due to nanoscale sharpness while still maintaining high current densities. In addition to their durability as emitters, carbon nanomaterials can be readily intercalated with other materials such as alkali metals to decrease the work function and thereby increase electron emission current.[5,7,8,18,19]

Carbon nanotubes possess excellent thermal transport and optical absorption properties,[20,21] making them suitable for use in thermionic and photoemission.[19] Graphene shares many of these beneficial properties such as high mechanical strength, thermal and electrical conductivity, and optical absorption.[22] Catalyst-free chemical vapor deposition methods for synthesizing graphitic petals on a number of substrates have been developed[12] and allow for relatively uniform and dense structures, as well as high optical absorptivity.[23] Moreover, the presence of many edges in this type of structure can be beneficial for emission, as edges have been shown to play an important role in electron emission for both graphene[17] and carbon nanotubes.[24] In addition, the high surface area to volume ratio of the petals creates a reactive material that could be advantageous for further modification.[25] In particular, intercalation with alkali metals has been shown to significantly reduce the work function of graphitic materials.[26] Prior work indicates that carbon nanofibers intercalated with potassium can be stable to high temperatures[5] and that intercalated carbon nanotubes also have excellent thermionic and photoemission properties.[19]

Despite almost 100 years of photoemission studies, uncertainty remains regarding the contributions of physical characteristics such as emitter geometry[27] and surface effects.[28] The present work focuses on thermionic and photoemission, and the theories describing these are discussed in greater detail below. However, any work on electron emission should acknowledge the pioneering work of Fowler and Nordheim[29] in developing a theory for field emission. Indeed much of their work on field emission has led to a greater understanding of other emission mechanisms, and the present work draws heavily from their foundational theoretical development. The interested reader can find informative reviews of field emission in Gomer,[4] Gadzuk and Plummer,[30] and Jensen.[31] In this work, we investigate vertically oriented graphitic petal arrays that exhibit unusual electron emission characteristics under a combination of photonic and thermal excitation. These petals are formed from 5 to 25 layers of graphene by microwave plasma chemical vapor deposition (MPCVD) synthesis on electrode graphite. A modified photoemission theory is developed and shows excellent agreement with experimental measurements.

II. EXPERIMENTAL METHODS

A. Material synthesis and characterization

Electron emission from graphitic petals requires that the substrate be rigid enough to support a thin layer of petals and provide a conductive path for electrons to the emitter. For thermionic emission, the substrate and emitter must also be capable of withstanding temperatures in excess of 1000 K and will ideally have high thermal conductivity. For this reason, electrode graphite was chosen as the substrate. The electrode graphite was approximately 10 mm by 10 mm square with a nominal thickness of 2 mm. The graphitic petal growth process employed here was reported by Bhuvana *et al.*, and a detailed description of the synthesis process can be found elsewhere.[32] Further studies[33] have shown that these petals, consisting of 5–25 layers of graphene, can be grown without a separate catalyst on a number of materials such as silicon, copper, and graphite. Figure 1 shows a typical scanning electron microscope (SEM) image of the plain electrode graphite before (a) and after (b) petal growth using the MPCVD system. Additionally, a transmission electron microscope image is provided in the supplemental section.[60] The growth of the petals is not entirely uniform across the sample surface. The plasma tends to couple best to the edges of the sample, and growth in these areas is densest. Multiple layers of petals could form in these dense areas around the edge.

Bulk graphite has a unique lamellar structure composed of layers of graphene with relatively weak interplanar interactions.[34] This structure makes it a favorable candidate for intercalation where atoms or compounds of another material are inserted between graphene layers. The process has been studied extensively for bulk graphite with a number of different materials known as graphite intercalation compounds. Much like semiconductor doping, the materials can be broken into the two basic categories: donors and acceptors.[26] However, unlike semiconductor doping where the dopant often occupies

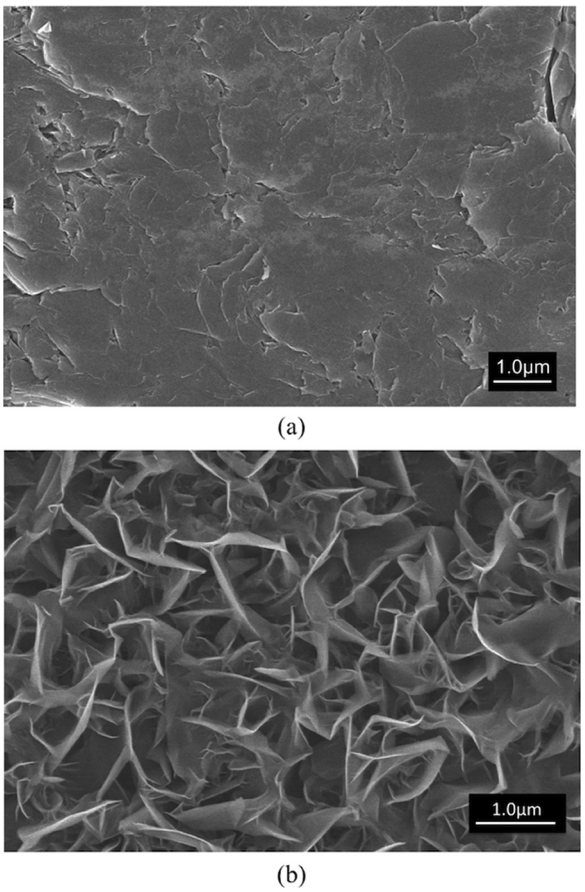

FIG. 1. (a) SEM image of the electrode graphite substrate prior to growing graphitic petals (b) Typical SEM image of few layer graphitic petals grown on an electrode graphite substrate.

a site in the semiconductor lattice when electrically active,[35] the intercalant occupies the space between atomic layers. Alkali metals are common donor intercalants,[26] and surface coating monolayers of alkali metals have been widely used to decrease the work functions of various metals.[36] Potassium was chosen in this work because it has been studied extensively in the literature and therefore provides a foundation for comparison. Potassium's efficacy as an intercalant is due to steric considerations as the potassium atoms fit well within the graphitic lattice.[37] Moreover, potassium-intercalation has been effective with other nanoscale carbon materials such as carbon nanotubes[38] and nanofibers.[5]

The process used to intercalate graphitic petals is based on a simple two-phase procedure described in prior work.[19] The sample and potassium were sealed in a custom-made borosilicate glass tube sealed with a Kovar fitting. In order to prevent oxidation from adsorbed water on the sample surface, all samples were heated at 560 K for 20 min in an argon glove box. The samples were then loaded into an intercalation vessel while still hot to prevent unwanted gases from adsorbing to the surface. X-ray diffraction (XRD) was performed on samples after emission testing at room temperature. The sample was quickly tested after being removed from vacuum to limit oxidation, and the XRD matched well to stage-1 potassium-intercalation. However, in the case when the sample was left in ambient conditions for an extended period of time, potassium peroxide (K_2O_2)

dominated the XRD spectrum. Figure 2(a) shows the results for a sample tested immediately after being removed from the vacuum chamber. The peak at 16.75° indicates stage-1 intercalation. Figure 2(b) shows XRD analysis on a sample that was left in ambient conditions for several hours. In this case, the peaks correspond to K_2O_2 peaks from JCPDS Card 76-2140.

Potassium-intercalated graphitic petals on a silicon substrate were also tested by XRD before being emission tested and results showed stage-1 intercalation. These results are similar to those from the intercalated graphitic petals on electrode graphite measured after emission testing thereby demonstrating that testing at lower temperatures (before deintercalation) does not drastically change the stage. The petal coated silicon substrate sample also indicates that the petals themselves are intercalated, thereby highlighting the importance of the surface structure over the bulk substrate.

B. Photo-excitation and electron energy measurements

The measurement system has been described in detail elsewhere,[19,24,39,40] and additional information is supplied in the supplementary material.[60] Briefly, the sample was placed in a high-vacuum environment on a stage with a built-in heater and bias supply. A hemispherical energy analyzer (HEA) located above the sample was used for measuring electron emission intensity as a function of the kinetic energy of emitted electrons. Several different light sources were used in this study; the main photo-excitation source was a Newport solar simulator (Model 69907 power supply and Model 67005 lamp box) with a xenon lamp (Model 6255 bulb) and an AM1.5 global filter (Model 81094). This source is designed to mimic solar radiation incident on the surface of the earth at an angle of 45°. Neutral density filters (Thorlabs Kit NDK01) were used to control the intensity of photonic illumination from a solar simulator during photoemission studies. In addition to the solar simulator, high power light emitting diodes (LEDs) were used for more monochromatic light sources. Two different LEDs were acquired, a blue LED (Thorlabs Model M470L2) and a green LED (Thorlabs Model M530L2). The full width at half maximum (FWHM) of the blue LED spectrum was 29 nm or 0.169 eV with peak intensity at 2.694 eV, while the FWHM of the green LED was 31 nm or 0.141 eV with a peak at 2.382 eV.

III. ELECTRON ENERGY DISTRIBUTION MODELING

Thermionic emission theory is well established, and elements of it are included here to facilitate comparison with photoemission models. We assume that the electron ensemble behaves to first order as a free electron gas. While this assumption is questionable for a nanoscale emitter, such as the thin graphitic petals used in this study, previous work has shown that it provides good fits for potassium-intercalated carbon nanotubes[19] and potassium-intercalated carbon nanofibers.[5] A second assumption is that the material has a single parabolic conduction band. Further investigation of the electronic structure, including detailed calculations of the energy bands could yield additional insight into the emission mechanism. However, this type of analysis is beyond the scope of this work, and the parabolic band assumption is often applied successfully to field emission from ultra-sharp emitter tips[41] including graphitic materials.[15]

With these assumptions in place, the number of thermally emitted electrons with energy between E and $E + dE$ and velocity in the z-direction (i.e., normal to the surface) incident on the surface per unit time per unit area can be calculated as[30,42]

$$I_{TEED} = \frac{4\pi m_e}{h^3} \frac{(E - E_F - \phi)H(E - E_F - \phi)}{1 + \exp\left(\frac{E-E_F}{k_B T}\right)} dE, \quad (1)$$

where m_e is the electron rest mass, E_F is the Fermi energy, ϕ is the work function, k_B is Boltzmann's constant, h is Planck's constant, T is temperature, and H represents the Heaviside step function used in the Richardson approximation.

The mechanism that underlies photoemission is generally more complicated to model. The advanced approaches used in prior literature, such as the three-step model, require detailed knowledge of the emitter geometry, band structure, and optical properties,[2,43] quantities not known in this study.

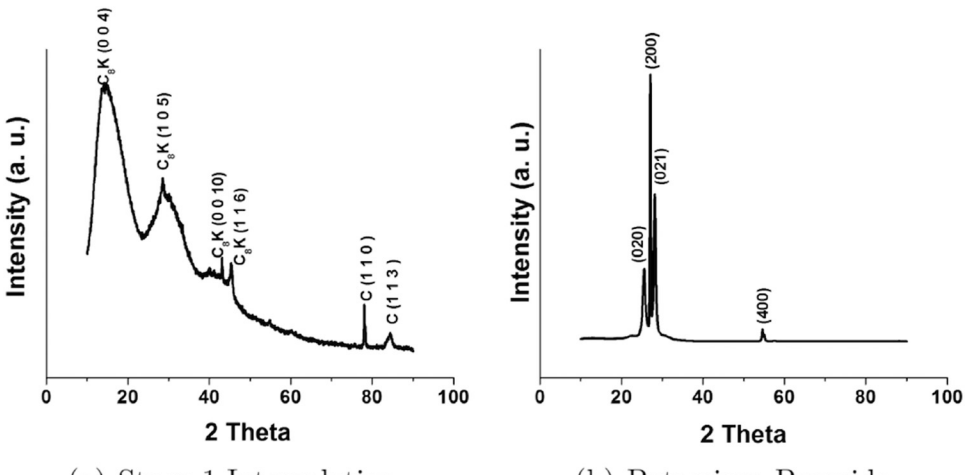

FIG. 2. XRD analysis performed on potassium-intercalated petals immediately after the sample underwent low temperature emission testing. The results for (a) are consistent with stage-1 intercalation, demonstrating that the sample maintained its intercalation staging throughout the testing. Spectrum (b) indicates that the sample has oxidized in the ambient environment.

Instead this work follows that of Fowler[29] and DuBridge[44] as a basis. The Fowler-Dubridge model has been successfully applied to experimental results from a previous study with potassium-intercalated carbon nanotubes.[5] To first order, the electron energy distribution (EED) for thermionic emission can be adjusted assuming the normal energy W of the electron population in the material is increased by the photon energy $\hbar\omega$, such that

$$I_{PEED} = \frac{4\pi m_e}{h^3} \frac{(E - E_F - \phi)H(E - E_F - \phi)}{1 + \exp\left(\frac{E - E_F - \hbar\omega}{k_B T}\right)} dE. \quad (2)$$

A number of assumptions underlie this model. First, following the thermionic model, a free-electron material with a single parabolic band is assumed. Second, the probability of an electron absorbing a photon is assumed to be independent of photon energy. Third, photon energy is entirely manifested as momentum in the normal direction. This last assumption is not physical; however, for examining the high-energy tail when the photon energy and work function are comparable, this assumption yields reasonable results because in order for an electron to emit when $\phi \approx \hbar\omega$, nearly all photon energy must manifest itself in the normal direction.[19]

The present work uses a broad-spectrum solar simulator. In such cases, a substantial fraction of photon energies greatly exceed the work function of the emitting material, such that not all photon energy must be converted to the normal direction for emission to occur. This discounts the assumption used in the derivation of Eq. (2). A random energy model is therefore developed instead following Jensen[1,45] and Westover[39] to account for the angle of incidence for photons. An expression $N_{avail,\Delta\theta p}$ for the number of electrons incident on the surface within the angle $\Delta\theta_p$ and with sufficient energy to emit can be developed. The expression weights the emission intensity generated by photons illuminated within the angle $\Delta\theta_p$ and the terms in I_{PEED} must be altered accordingly. The total EED is then described by

$$I_{PEED}(E)dE = \sum_{n=1}^{N} \frac{N_{avail,\Delta\theta_p}(\theta_p)\Delta\theta_p}{N_{avail,total}} I_{PEED,\Delta\theta_p}(E)dE, \quad (3)$$

where $I_{PEED,\Delta\theta p}$ is as follows:

$$I_{PEED,\Delta\theta_p} = \frac{4\pi m_e}{h^3} \frac{(E - E_F - \phi)H(E - E_F - \phi)}{1 + \exp\left(\frac{E - E_F - \hbar\omega\cos(\theta_p)}{k_B T}\right)} dE. \quad (4)$$

The total number of incident electrons can be found by summing over all intervals of $\Delta\theta_p$ such that

$$N_{avail,total} = \sum_{n=1}^{N} N_{avail,\Delta\theta_p}(\theta_P). \quad (5)$$

Equations (3) and (4) are referred to in this document as the "random energy" photoemission model, while Eq. (2) is termed the "normal energy" photoemission model. Both can be considered to be variants of the Fowler-Dubridge model.

IV. RESULTS AND DISCUSSION

Two samples were tested in this study. Both samples consisted of potassium-intercalated petals grown on electrode graphite and were prepared in the same manner, but several months apart. Figure 3 shows normalized thermionic EEDs (TEEDs) from plain graphitic petals and potassium-intercalated graphitic petals (sample 1). The characterization of emission from the graphitic substrate and plain petals is not discussed at length here because their relatively high work functions (4–5 eV) limits the amount of incident radiation from the solar spectrum that has sufficient energy to directly photoemit an electron from the material. Therefore, most non-intercalated petal emission results are from thermionic studies and are provided in the supplemental material.[60] TEEDs of plain petals indicated a work function of 4.6 eV, while TEEDs of intercalated petals produced work functions as low as 2.2 eV, where the difference is taken between the maximum peak intensities. Thermionic emission from the plain petals is negligible below 1123 K but temperatures above 673 K would promote deintercalation of the potassium-intercalated petals. Therefore, two different temperatures are used for the TEED measurements shown in Figure 3.

The addition of graphitic petals to a plain graphite surface generates a very large increase in intensity relative to plain graphite (20%–100%), suggesting that the petals increase the photon absorbance.[25] Furthermore, the resulting EEDs for intercalated petals is narrower than the EEDs for non-intercalated. Robinson *et al.* also observed narrowing of the distribution with graphite fibers, and suggested that it could be due to a hybridized state between the nearly free electron state of the graphite and an *s* state of the potassium.[5] Given the significant increase in emission intensity for low-temperature photo-excited petals, the intercalation of graphitic petals provides a superior emitter material. In terms of prospective energy conversion applications, a high-intensity, broad distribution is advantageous because the total current is given by the integral of the emission intensity. Unfortunately, photo-excited EEDs resulting from broadband illumination had a much narrower distribution than that expected from the random energy model. Figure 4 shows

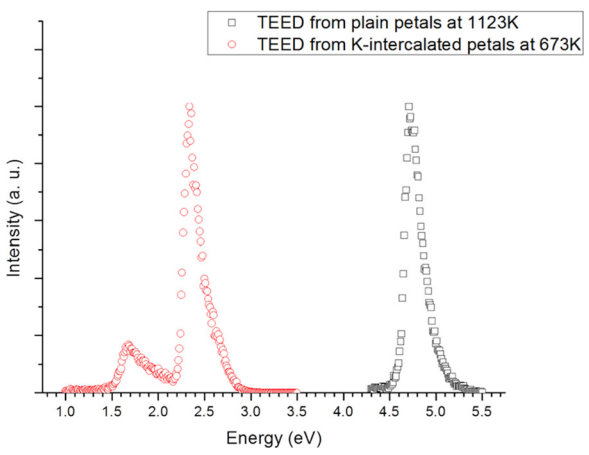

FIG. 3. TEEDs of graphitic petals on electrode graphite before and after potassium-intercalation (sample 1).

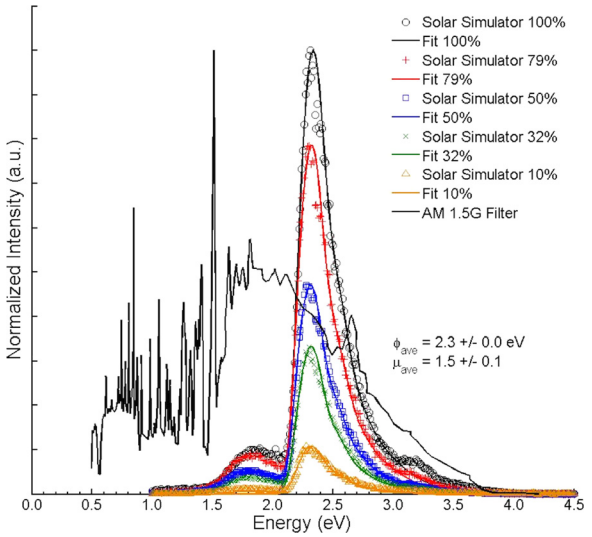

FIG. 4. Measured EEDs from potassium-intercalated graphitic petals (sample 1) at 310 K due to photo-excitation with the solar simulator. Fits correspond to random energy photoemission theory with phonon scattering contributions.

EEDs from sample 1 prior to heating. Photoemission fits utilizing a modification of the random energy model are also plotted. The random energy model was modified to include scattering of electrons and details of this theoretical modification are given below.

EEDs of the photo-excited samples were narrow relative to the random energy model fits. In fact, better theoretical fitting to the experimental data can be obtained by simply using thermionic theory. However, the resulting fitted temperatures are much greater than the actual lattice temperatures and do not account for the energy contributions from photon absorption making the fits invalid. These fitting comparisons are demonstrated clearly in the supplemental material.[60] Narrowed distributions may result from electrons being scattered by phonons, causing higher energy electrons to emit at lower energies. Following recent work by Sun *et al.*, these scattering effects can be incorporated into the present photoemission theory.[46] Several assumptions are invoked. First, electrons are scattered by optical phonons, with equal probability, and each scattering event results in a reduction of electron energy equal to the phonon energy. Second, the probability of an electron scattering n times and still emitting given a mean number of scattering events μ, follows a Poisson distribution. Based on these assumptions, the photoemission theory modified to account for scattering of electrons by optical phonons is given by

$$I_{SCAT}(E)dE = \sum_{n=0}^{m} C(n)\frac{\exp(-\mu)}{n!}\mu^n I_{PEED}(E + nE_{ph})dE, \quad (6)$$

$$C(n) = \left[\sum_{j=0}^{n} \exp(-\mu)\frac{\mu^j}{j!}\right]^{-1}, \quad (7)$$

where n is the number of scattering events, E_{ph} is the phonon energy, μ is the mean number of scattering events that emitted electrons experience, $C(n)$ is a probability normalization coefficient and $I_{PEED}(E + nE_{ph})$ is the photoemission intensity calculated by the random energy model. E_{ph} is taken to be 0.21 eV based on the high energy optical phonon in the graphene band structure.[47] Assuming that a negligible number of electrons with energy greater than $\hbar\omega_{max}$ will emit, m is the maximum integer value such that $E + mE_{ph} \leq \hbar\omega_{max}$.

TABLE I. Parameter values from data fitting to EEDs in Figure 4 generated by solar simulator illumination of potassium-intercalated graphitic petals (sample 1).

Optical intensity (%)	Work function (eV)	μ	RMSE (eV)
100	2.3	1.6	0.044
79	2.3	1.4	0.048
50	2.3	1.7	0.053
32	2.3	1.6	0.053
10	2.3	1.4	0.062

In Figure 4, the light intensity of the photo illumination on sample 1 is varied and each EED is normalized with respect to the EED resulting from 100% illumination by the solar simulator. The normalized photon flux from the AM1.5 G filter is plotted for comparison. The average, fitted work function from the EEDs is 2.3 ± 0.1 eV, the average mean number of scattering events is 1.5 ± 0.1, and the average root mean squared error (RMSE) of the plots is 0.052 ± 0.007 eV. Table I provides the parameter values for every intensity of solar illumination. Parameter values do not fluctuate significantly with changes in optical intensity. A low-energy leading edge is apparent in the measured EEDs just prior to the main emission peak suggesting that the sample has a small area with an even lower work function potentially resulting from surface adsorbed potassium.

Thermal effects were evaluated in sample 1 by varying the base temperature of the emitter samples via a controlled, heated stage. Figure 5 shows the mean scattering events for a given lattice temperature plotted against optical intensity (with respect to 1 sun of illumination from the solar simulator). The reported values are averaged from 3 to 4 fitted EEDs over the course of 4 heating and cooling cycles, and standard deviations are included with each data point. Table II provides

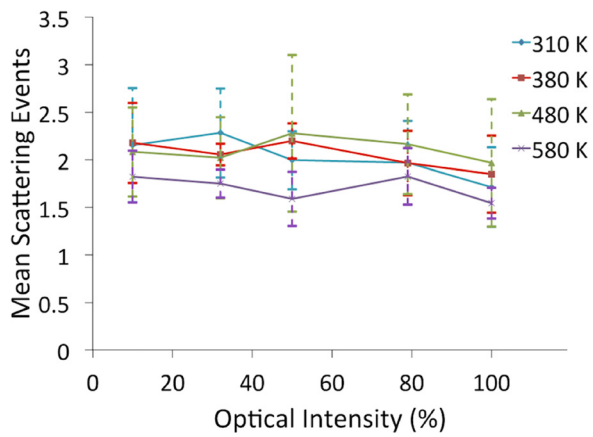

FIG. 5. Mean scattering events experienced by emitted electrons of potassium-intercalated graphitic petals (sample 1) calculated by fitting theory to measured EEDs and plotted as a function of illumination intensity.

TABLE II. Resulting integrals of EEDs (# electrons • eV) evaluated for Figure 5 from potassium-intercalated graphitic petals (sample 1) measurements.

Optical intensity (%)	310 K	380 K	480 K	580 K
100	3.3×10^3	4.0×10^3	3.7×10^3	3.6×10^3
79	2.5×10^3	3.0×10^3	2.7×10^3	2.8×10^3
50	1.6×10^3	1.8×10^3	1.9×10^3	1.7×10^3
32	1.1×10^3	1.3×10^3	1.2×10^3	1.2×10^3
10	0.4×10^3	0.4×10^3	0.4×10^3	0.4×10^3

average values for the integrals of the EEDs (total emission intensity) shown in Figure 5. The reduction in emission intensity matches very closely with the reduction in solar illumination. A significant variation exists in the number of scattering events, with most values in the range of 1.5–3.5. A subtle overall trend exists amongst the averaged data points of decreasing scattering events with increasing illumination intensity, though significant standard deviations generate a wide range of inaccuracy. This counterintuitive result suggests that an increase in emission intensity causes less electron scattering among emitting electrons. Additionally, there appears to be a consistent decrease in scattering at 580 K at all illumination intensities despite a negligible change in emission intensity relative to the other temperatures. This may be a result of physical changes in the sample such as oxide burn off, discussed in greater detail in the supplemental materials section.[60]

Another approach to characterizing the EEDs is to examine how the FWHM varies. Figure 6 contains a plot of FWHM as a function of optical intensity (with respect to 1 sun of illumination) for several substrate temperatures of sample 1. The plot on the left was generated after 2 heating cycles up to 580 K and subsequent cooling to room temperature. The plot on the right was generated after the sample had cooled from the measurements on the left plot. A clear trend of increasing FWHM with optical intensity is present. This effect occurs most prominently at room temperature, particularly with the plot on the left. These results parallel the decrease in scattering events with increasing optical intensity that were derived from data fitting, as fewer scattering events result in a broader distribution.

Electron-phonon coupling in graphene has been studied as a function of doping density, both theoretically[48–50] and experimentally.[51–55] Transient absorption microscopy studies have observed a relatively slow decay (1.4 ps) in suspended graphene, compared to substrate-supported graphene (~200 fs), with the slow decay component attributed to hot phonon effects.[54] This is generally consistent with Raman spectroscopy results at moderate carrier densities, which indicate that the electron-phonon coupling weakens with increasing doping.[55] For high levels of potassium doping, the Raman G-peak can split, indicating inhomogeneous doping, and to soften and broaden, indicating a reduction of phonon lifetimes with increasing doping (with respect to corresponding values at low carrier densities).[55] Comparable behavior is observed in samples with 1–4 layers of graphene, indicating that the layers are weakly coupled. This suggests that having thin petals will result in a slower electron energy decay allowing for an increase in emission intensity and electron energy as the electrons will have a longer time to emit before they lose their energy. The increasing FWHM in Figure 6 may be a result of weakened electron-phonon coupling as higher energy electrons are allowed to emit.[56] Moreover, an increase in the average energy of the emitted electrons will cause a broadening of the EED and a possibly a positive net energy exchange leaving the sample that would generate a cooling effect within the sample, further decreasing electron-phonon coupling. In such a scenario, a superlinear increase in FWHM will occur with increasing optical intensity as lattice cooling and electron-phonon decoupling effects intensify.

Sample 2 demonstrated large shifts in work function, scattering events, and overall EED shape as it went through heating cycles. These shifts can likely be attributed to deintercalated potassium, potassium oxide burn-off, and extremely high electron counts. This phenomenon can subsequently have a negative impact on the work function of the detector as well. Due to the reactive nature of the samples tested, it was not possible to remove them from the chamber in order to recalibrate the detector. However, with narrowband illumination from LEDs, direct photoemission can be used for calibration. With known peaks and FWHMs, sample emission from LED excitation can be used to calibrate the analyzer work function in real time. To do this, an LED induced EED is chosen, and the energy is allowed to shift when fitting the theoretical model to the EED. The analyzer work function can then be adjusted by the amount of the shift in energy. LED emission is very appealing as an *in situ* calibration method; however, the material must have a sufficiently low work function for this method to be viable with the green and blue LEDs utilized in this effort.

Figure 7 contains plots from the first heating cycle of sample 2 comparing normalized photo-excited EEDs from both solar simulator and LEDs. Solar illuminated samples

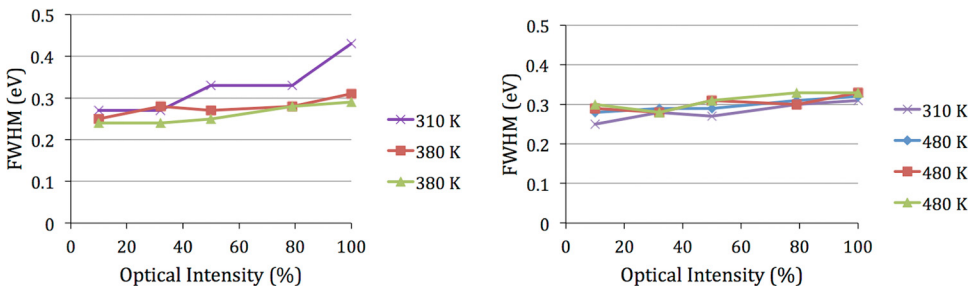

FIG. 6. FWHM of measured EEDs versus optical intensity generated after potassium-intercalated graphitic petals (sample 1) experience two heating cycles up to 580 K and cooled (left) and after the sample has then been again heated to 380 K and cooled (right).

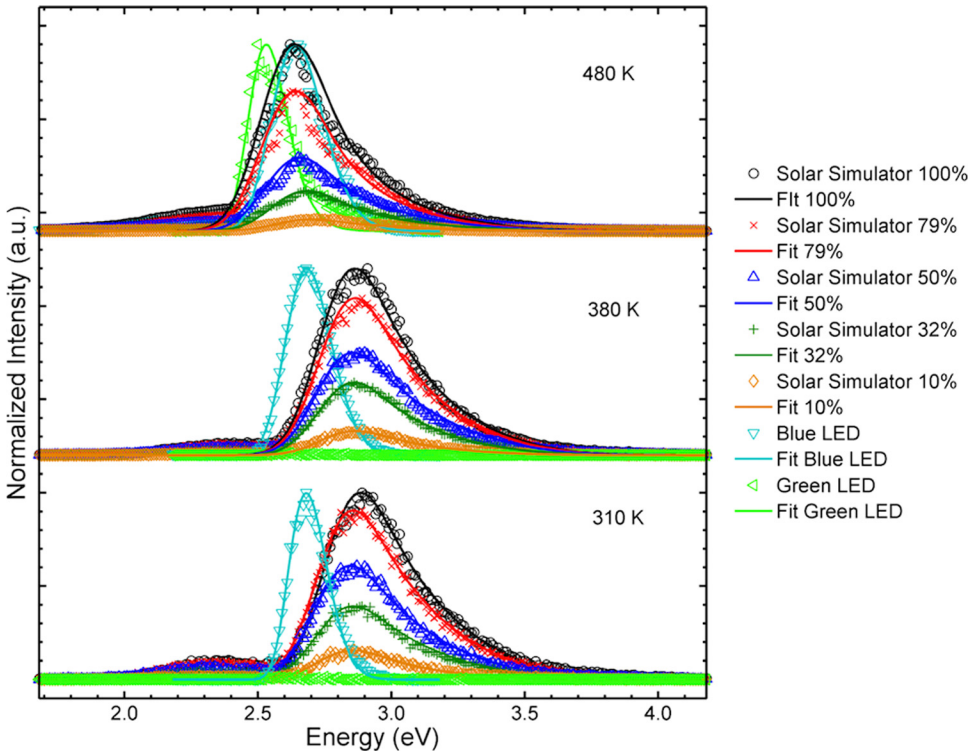

FIG. 7. Normalized EEDs measured from potassium-intercalated graphitic petals (sample 2) illuminated with solar simulator and blue/green LEDS for temperatures of 310 K, 380 K, and 480 K.

are normalized with respect to the EED corresponding to 100% solar illumination while LED induced EEDs are normalized by their own peak intensity. Negligible thermionic emission occurs prior to 580 K and thus is not shown. The data fitting results, using the random energy photoemission theory with phonon scattering contributions, of all EEDs from solar simulator illumination for a given temperature are presented in Table III. A reduction in work function occurs with increasing temperature as indicated by the results given in Table III and which is further demonstrated by the plots in Figure 7 in which the green LED does not produce a measurable EED until after the sample has been heated to 480 K suggesting that the work function of the sample was not low enough for excitation to occur via green LED illumination prior to heating. An increase in maximum emission intensity of greater than thirty times occurs between 310 K and 480 K despite only a three times increase expected from theory by the lowering of work function and increase in temperature. This result suggests that chemical changes are occurring within the sample, such as potassium oxidation burn-off and increased intercalation, thereby increasing the overall area of the sample emitting low energy electrons. Above 480 K, emission counts decreased significantly and multiple work functions were demonstrated via multiple peaks in the EEDs. While the emission counts are reduced, a further reduction in work function does occur when heated up to 680 K as demonstrated in the supplemental material section.[60] The reduction in work function may be a result of deintercalated potassium forming on the surface of the sample, though it is more likely that further removal of oxides on the surface of the sample is the cause.

TABLE III Parameter values from data fitting to EEDs generated by solar simulator illumination of potassium-intercalated graphitic petals (sample 2).

Temperature (K)	Optical intensity (%)	Work function (eV)	μ	RMSE (eV)
310	100	2.7	1.2	0.037
310	79	2.7	1.3	0.038
310	50	2.7	1.3	0.039
310	32	2.7	1.3	0.041
310	10	2.7	1.7	0.044
380	100	2.7	1.5	0.027
380	79	2.7	1.4	0.030
380	50	2.7	1.2	0.031
380	32	2.7	1.6	0.028
380	10	2.7	1.7	0.030
480	100	2.5	2.1	0.052
480	79	2.5	2.0	0.053
480	50	2.5	1.6	0.046
480	32	2.5	1.6	0.043
480	10	2.6	1.2	0.044

The petals utilized in this study are comprised of 5–25 layers of graphene, and they differ from graphene due to a slight overlap of the bands at the Fermi-level that cause them to be a semi-metal as opposed to a zero band gap semiconductor.[22,34] In addition, the petals are not completely planar. Rippling of graphene sheets has been suggested to cause rehybridization between the π and σ orbitals in the graphene band.[57] However, in many respects, the graphite band structure is qualitatively similar to graphene, and therefore, examining the graphene electronic band structure can provide insight into how the work function of the intercalated petals is reduced. In the graphene band structure an energy change of approximately 2.7 eV separates the K-point (Dirac point) from the M-point (saddle point).[17,58] The saddle point is expected to exhibit a very high density of states although calculations vary depending on the hopping parameter, t.[59] Consequently, it would be difficult to raise the Fermi-level

above the saddle point.[22] However, most electronic studies of graphene focus on the K-point, and therefore, accurate calculations of the band structure at higher energies are less developed. Nevertheless, the distance between the K- and M-points in the graphene band structure matches very closely to the shift in work function measured between plain and intercalated petals. Therefore, initial results from potassium-intercalated graphitic petals suggest that emitting electrons originate near the saddle point in the graphite/graphene band structure. More detailed analysis on the band structure could yield improved results on the understanding of both the band structure of C_8K (stage-1 intercalation) as well as emission from a saddle point.

V. CONCLUSIONS

Electron emission from graphitic nanopetals was investigated using a HEA. Potassium-intercalation of graphitic petals dramatically changes the measured EED. The nature of the intercalation was investigated using XRD and Raman analysis (presented in the supplemental materials section),[60] which showed stage-1 intercalation was consistently obtained. This intercalation provides the highest ratio of potassium to carbon, and should produce the largest charge transfer and hence lower the work function. Emission from intercalated samples was compared to emission from samples without intercalation and the results indicate that intercalation not only lowers the work function by 2.4–2.8 eV but can also lead to emission from multiple work functions. The potassium-intercalated graphitic petals are a complex structure, and the stability of their photo-excited emission for varying temperatures was investigated. The material was found to be relatively stable at lower temperatures (<480 K) but was unstable at higher temperatures (>580 K). This instability is attributed to potassium-oxide burn-off and the increased mobility of the potassium atoms within the graphite lattice with increased temperature leading to deintercalation.

A random energy photoemission model was developed and modified to account for electron scattering. This model was effectively used for quantitative fitting of theory to the experimental photoemission EEDs when pure thermionic and photoemission theories were not suitable. The resulting fits indicate that electron scattering by optical phonons does account for a lowering of emission energy and a narrowing of the EED. The relative intensity of these peaks was observed to change with temperature further suggesting that the sample undergoes modification in structure at elevated temperatures. The increased surface area of the petals relative to bulk graphite and their large number of defects make the petals highly reactive and non-uniform. However, this non-uniformity provides a good emission source. Unfortunately, the narrowing of the EEDs caused by the scattering of electrons limits the range of energies that could be used in an energy conversion device. However, this does not offset the gain in emission intensity that is induced by the reduced work function. These factors, and the simplicity of the sample preparation, including petal growth and intercalation, make this process amendable to practical devices.

ACKNOWLEDGMENTS

The authors thank Tianyin Sun and Robert Nemanich for their assistance with implementing scattering effects into the random energy model. The authors would also like to thank Oliver Jezuit and Kevin McMullen for their training and collaborations with equipment utilized for the work presented.

[1]K. L. Jensen, J. Appl. Phys. **102**, 024911 (2007).
[2]M. Cardona and L. Ley, *Photoemission in Solids I: General Principles* (Springer-Verlag, Berlin, New York, 1978).
[3]E. L. Murphy and R. H. Good, Phys. Rev. **102**, 1464 (1956).
[4]R. Gomer, *Field Emission and Field Ionization* (Harvard University Press, Cambridge, 1961).
[5]V. S. Robinson, T. S. Fisher, J. A. Michel, and C. M. Lukehart, Appl. Phys. Lett. **87**, 061501 (2005).
[6]F. A. M. Koeck and R. J. Nemanich, J. Appl. Phys. **112**, 113707 (2012).
[7]Y. Saito and S. Uemura, Carbon **38**, 169 (2000).
[8]U. A. Palnitkar, R. V. Kashid, M. A. More, D. S. Joag, L. S. Panchakarla, and C. N. R. Rao, Appl. Phys. Lett. **97**, 063102 (2010).
[9]W. A. Deheer, A. Chatelain, and D. Ugarte, Science **270**, 1179 (1995).
[10]P. Liu, Y. Wei, K. L. Jiang, Q. Sun, X. B. Zhang, S. S. Fan, S. F. Zhang, C. G. Ning, and J. K. Deng, Phys. Rev. B **73**, 235412 (2006).
[11]C. H. Weng, K. C. Leou, H. W. Wei, Z. Y. Juang, M. T. Wei, C. H. Tung, and C. H. Tsai, Appl. Phys. Lett. **85**, 4732 (2004).
[12]Y. H. Wu, B. J. Yang, B. Y. Zong, H. Sun, Z. X. Shen, and Y. P. Feng, J. Mater. Chem. **14**, 469 (2004).
[13]S. Dumpala, A. Safir, D. Mudd, R. W. Cohn, M. K. Sunkara, and G. U. Sumanasekera, Diamond Relat. Mater. **18**, 1262 (2009).
[14]S. Wang, J. Wang, P. Miraldo, M. Zhu, R. Outlaw, K. Hou, X. Zhao, B. C. Holloway, D. Manos, T. Tyler, O. Shenderova, M. Ray, J. Dalton, and G. McGuire, Appl. Phys. Lett. **89**, 183103 (2006).
[15]G. Eda, H. E. Unalan, N. Rupesinghe, G. A. J. Amaratunga, and M. Chhowalla, Appl. Phys. Lett. **93**, 233502 (2008).
[16]Z.-S. Wu, S. Pei, W. Ren, D. Tang, L. Gao, B. Liu, F. Li, C. Liu, and H.-M. Cheng, Adv. Mater. **21**, 1756 (2009).
[17]Z. Xiao, J. She, S. Deng, Z. Tang, Z. Li, J. Lu, and N. Xu, ACS Nano **4**, 6332 (2010).
[18]V. S. Robinson, Y. Show, G. M. Swain, R. G. Reifenberger, and T. S. Fisher, Diamond Relat. Mater. **15**, 1601 (2006).
[19]T. L. Westover, A. D. Franklin, B. A. Cola, T. S. Fisher, and R. G. Reifenberger, J. Vac. Sci. Technol. B **28**, 423 (2010).
[20]P. Avouris, M. Freitag, and V. Perebeinos, Nature Photon. **2**, 341 (2008).
[21]Z.-P. Yang, L. Ci, J. A. Bur, S.-Y. Lin, and P. M. Ajayan, Nano Lett. **8**, 446 (2008).
[22]A. H. Castro Neto, F. Guinea, N. M. R. Peres, K. S. Novoselov, and A. K. Geim, Rev. Mod. Phys. **81**, 109 (2009).
[23]B. Duyvuri, A. Kumar, H. Bao, H. Huang, T. Fisher, and X. Ruan, in *Proceedings of the ASME 2010 3rd Micro/Nanoscale Heat & Mass Transfer International Conference* (Atlanta, GA, 2012), Paper No. MNHMT2012–75228.
[24]A. G. Rinzler, J. H. Hafner, P. Nikolaev, L. Lou, S. G. Kim, D. Tomanek, P. Nordlander, D. T. Colbert, and R. E. Smalley, Science **269**, 1550 (1995).
[25]K. J. McMullen, MSME thesis, Purdue University, 2010.
[26]M. S. Dresselhaus and G. Dresselhaus, Adv. Phys. **51**, 1 (2002).
[27]M. Schenk, M. Krueger, and P. Hommelhoff, Phys. Rev. Lett. **105**, 257601 (2010).
[28]I. Adawi, Phys. Rev. A **134**, A1649 (1964).
[29]R. H. Fowler and L. Nordheim, Proc. R. Soc. London **119**, 173 (1928).
[30]J. W. Gadzuk and E. W. Plummer, Rev. Mod. Phys. **45**, 487 (1973).
[31]P. W. Hawkes and K. L. Jensen, Electron Emiss. Phys. **149**, IX (2007).
[32]T. Bhuvana, A. Kumar, A. Sood, R. H. Gerzeski, J. Hu, V. S. Bhadram, C. Narayana, and T. S. Fisher, ACS Appl. Mater. Interfaces **2**, 644 (2010).
[33]C. S. Rout, A. Kumar, and T. S. Fisher, Nanotechnology **22**, 395704 (2011).
[34]D. D. L. Chung, J. Mater. Sci. **37**, 1475 (2002).
[35]S. A. Campbell and Knovel (Firm), in *The Oxford Series in Electrical and Computer Engineering*, 3rd ed. (Oxford University Press, New York, 2008), p. xiv.
[36]L. Osterlund, D. V. Chakarov, and B. Kasemo, Surf. Sci. **420**, 174 (1999).

[37]W. A. Kamitakahara and H. Zabel, Phys. Rev. B **32**, 7817 (1985).
[38]J. J. Zhao, J. Han, and J. P. Lu, Phys. Rev. B **65**, 193401 (2002).
[39]T. L. Westover, Ph.D. dissertation, Purdue University, 2008.
[40]K. Uppireddi, T. L. Westover, T. S. Fisher, B. R. Weiner, and G. Morell, J. Appl. Phys. **106**, 043716 (2009).
[41]P. Deb, T. Westover, H. Kim, T. Fisher, and T. Sands, J. Vac. Sci. Technol. B **25**, L15 (2007).
[42]R. D. Young, Phys. Rev. **113**, 110 (1959).
[43]B. Feuerbacher, B. Fitton, and R. F. Willis, *Photoemission and the Electronic Properties of Surfaces* (Wiley, London, New York, 1978).
[44]L. A. DuBridge, Phys. Rev. **43**, 0727 (1933).
[45]K. L. Jensen, D. W. Feldman, N. A. Moody, and P. G. O'Shea, J. Appl. Phys. **99**, 124905 (2006).
[46]T. Sun, F. A. M. Koeck, C. Zhu, and R. J. Nemanich, Appl. Phys. Lett. **99**, 202101 (2011).
[47]D. Singh, J. Y. Murthy, and T. S. Fisher, J. Appl. Phys. **110**, 044317 (2011).
[48]C. H. Park, F. Giustino, M. L. Cohen, and S. G. Louie, Nano Lett. **8**, 4229 (2008).
[49]C. Attaccalite, L. Wirtz, M. Lazzeri, F. Mauri, and A. Rubio, Nano Lett. **10**, 1172 (2010).
[50]K. M. Borysenko, J. T. Mullen, X. Li, Y. G. Semenov, J. M. Zavada, M. B. Nardelli, and K. W. Kim, Phys. Rev. B **83**, 161402(R) (2011).
[51]M. Bianchi, E. D. L. Rienks, S. Lizzit, A. Baraldi, R. Balog, L. Hornekaer, and P. Hofmann, Phys. Rev. B **81**, 041403(R) (2010).
[52]D. K. Efetov and P. Kim, Phys. Rev. Lett. **105**, 256805 (2010).
[53]L. Huang, G. V. Hartland, L.-Q. Chu, Luxmi, R. M. Feenstra, C. Lian, K. Tahy, and H. Xing, Nano Lett. **10**, 1308 (2010).
[54]B. Gao, G. Hartland, T. Fang, M. Kelly, D. Jena, H. Xing, and L. Huang, Nano Lett. **11**, 3184 (2011).
[55]C. A. Howard, M. P. M. Dean, and F. Withers, Phys. Rev. B **84**, 241404(R) (2011).
[56]N. M. Miskovsky, S. H. Park, J. He, and P. H. Cutler, J. Vac. Sci. Technol. B **11**, 366 (1993).
[57]E.-A. Kim and A. H. Castro Neto, EPL **84**, 57007 (2008).
[58]T. Ohta, A. Bostwick, T. Seyller, K. Horn, and E. Rotenberg, Science **313**, 951 (2006).
[59]J. Gonzalez, Phys. Rev. B **78**, 205431 (2008).
[60]See supplemental material at http://dx.doi.org/10.1063/1.4805038 for further information regarding sample fabrication, potassium intercalation and oxidation, the experimental setup and detector calibration, thermionic emission data, and theoretical derivation and validation.